Inverse Rendering for High-Genus Surface Meshes from Multi-View Images

Supplementary Material

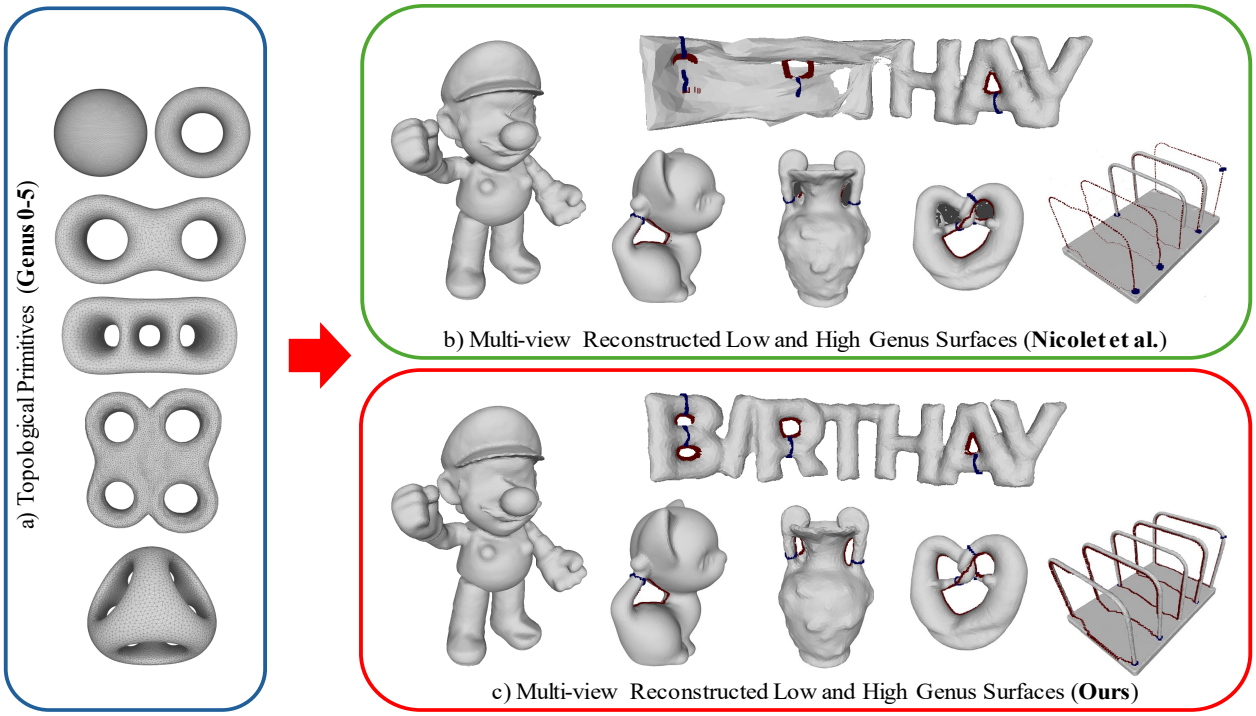

Figure 1. (a) Topological primitives that are homeomorphic to the ground truth surfaces, ensuring topological consistency. (b) Reconstructed 3D surface by minimizing the multi-view rendering loss using SOTA method [**?**]. (c) Reconstructed 3D surface using our method. The topological information of the ground truth is represented with tunnel loops shown in Red and handle loops in Blue for visual comparisons of topological features.

A1. Complete Qualitative Comparisons with Nicolet et al.[?] for Low-Genus Reconstruction

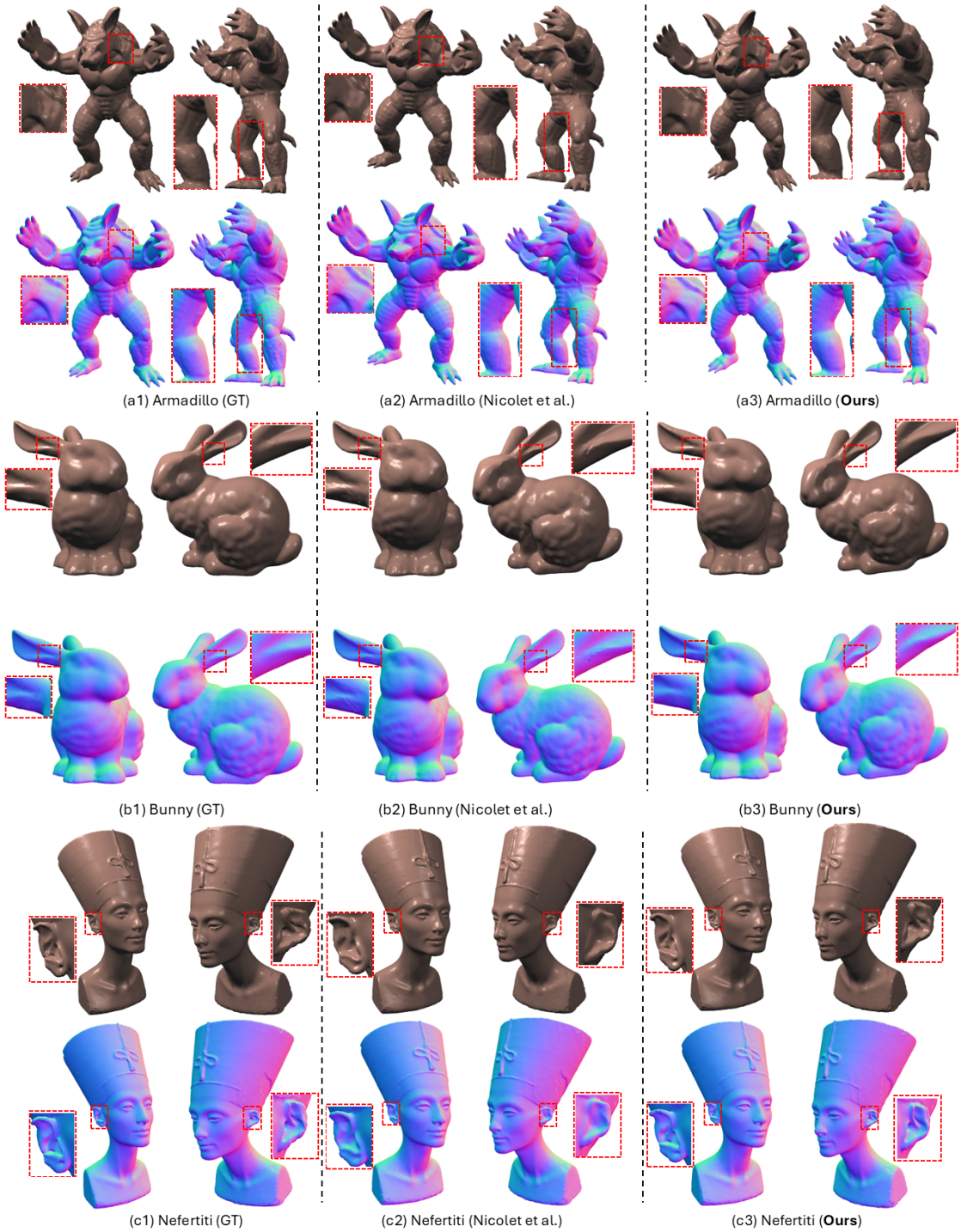

(a1) Armadillo (GT) (a2) Armadillo (Nicolet et al.) (a3) Armadillo (**Ours**)

(b1) Bunny (GT) (b2) Bunny (Nicolet et al.) (b3) Bunny (**Ours**)

(c1) Nefertiti (GT) (c2) Nefertiti (Nicolet et al.) (c3) Nefertiti (**Ours**)

Figure 1. Qualitative Comparisons with Nicolet et al. [**?**]: Multi-View Reconstruction of **Low Genus (Genus-0)** Surfaces using Rendered Views and Normal Maps with a **Sphere (Genus-0) as the Topological Primitive**.

A2. Complete Qualitative Comparisons with Nicolet et al.[?] for High-Genus Reconstruction

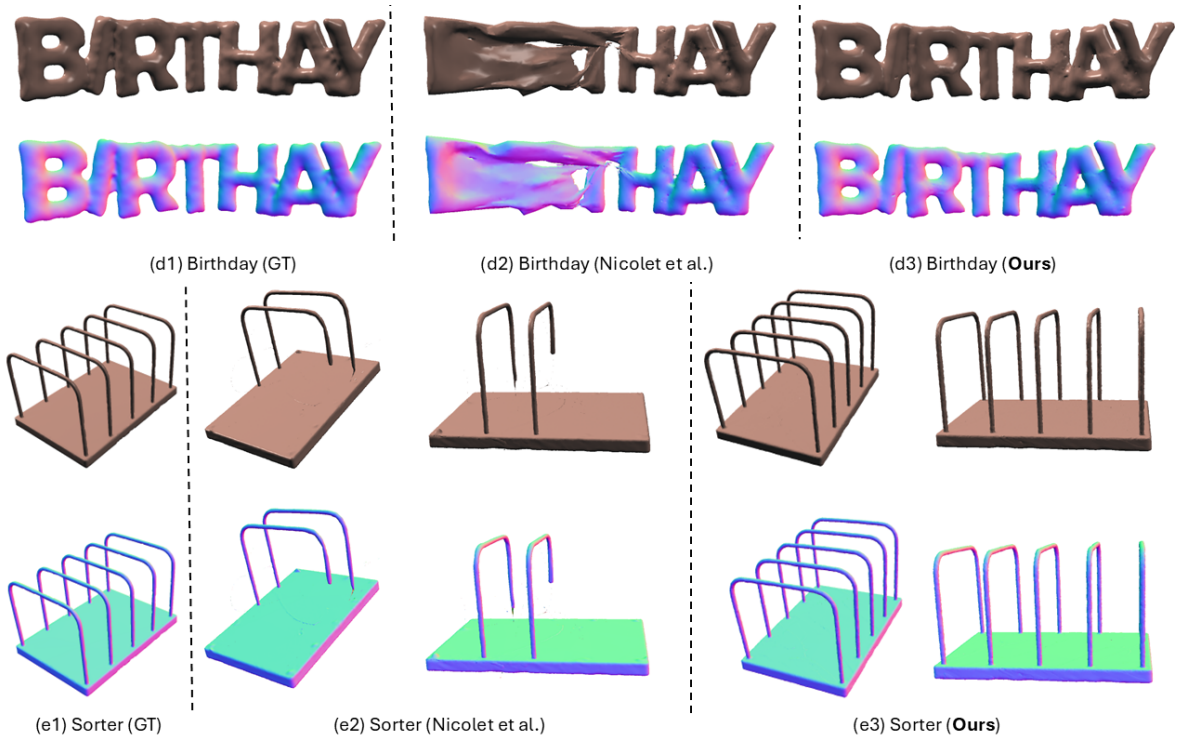

Figure 2. Qualitative Comparisons with Nicolet et al. [**?**]: Multi-View Reconstruction of **High-Genus (Genus 1-5)** Surfaces using Rendered Views and Normal Maps Using Topologically Consistent **Triangulated Primitives (Genus 1, 2, 3, 4 and 5 from top to bottom, respectively**).

B. How to Construct Topological Primitive of Any Genus g ?

Connected Sum: An Algebraic Topology Perspective

Definition (Connected Sum) [**?**]. The connected sum $S_1 \oplus S_2$ is formed by deleting the interior of disks D_1 and D_2 from the surfaces S_1 and S_2, respectively, and attaching the resulting punctured surfaces $S_1 - D_1$ and $S_2 - D_2$ to each other along their boundaries via a homeomorphism $h : \partial D_1 \to \partial D_2$ as shown in **Figure 3**. Mathematically, this can be expressed as:

$$S_1 \oplus S_2 = (S_1 - D_1) \cup_h (S_2 - D_2).$$

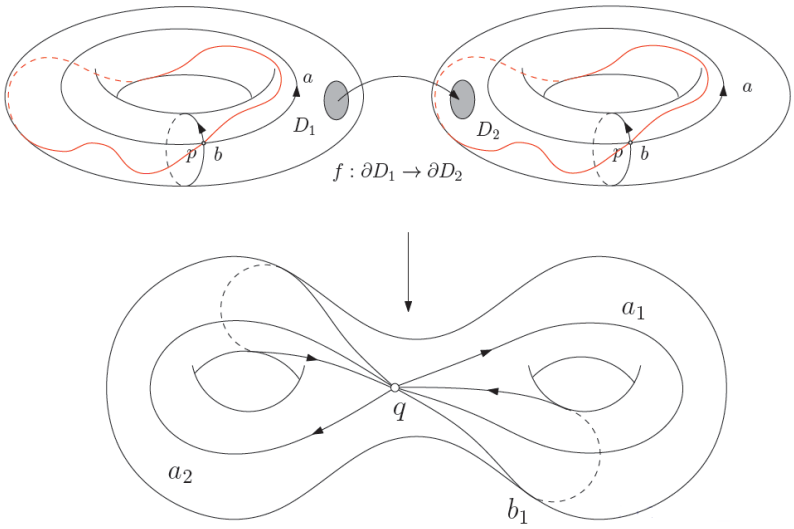

Figure 3. Two surfaces S_1 and S_2 are shown with disks D_1 and D_2 removed. These surfaces are then glued together along the boundary of the disks, resulting in a surface with a genus equal to the sum of the genera of S_1 and S_2.[**?**]

Steps for Constructing a Topological Primitive Using S_1 and S_2: Say S_1 and S_2 are surfaces with genus g_1 and g_2, respectively. Applying the definition of the direct sum provided earlier, a new surface $S_1 \oplus S_2$ of genus $g_1 + g_2$ can be readily constructed. By the properties of direct sums, the genus of $S_1 \oplus S_2$ satisfies:

$$\text{genus}(S_1 \oplus S_2) = \text{genus}(S_1) + \text{genus}(S_2) = g_1 + g_2.$$

Hence, we can construct complex topological primitatives of any **genus g** from the existing ones as illustrated in **Figure 4**.

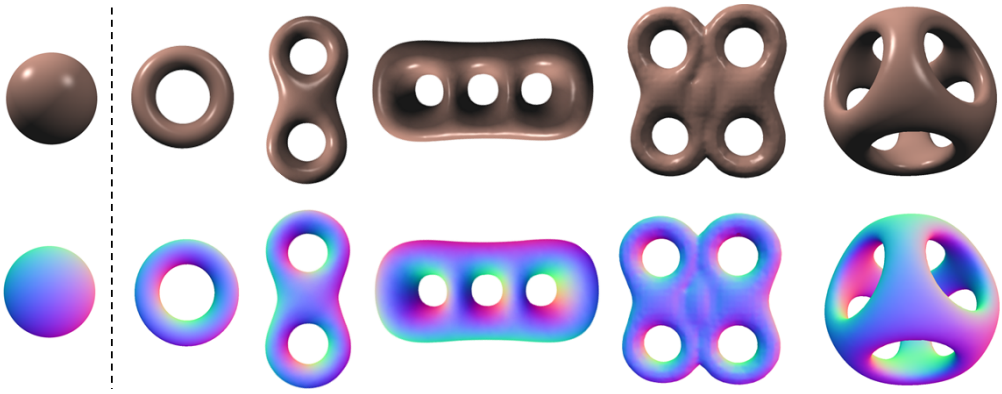

Figure 4. **Topological Primitives (genus 0–5).** Left to right: Sphere ($\mathbf{S_0}$, g=0), Torus ($\mathbf{S_1}$, g=1), Double ($\mathbf{S_2}$, g=2), Triple ($\mathbf{S_3}$, g=3), Quadruple Torus ($\mathbf{S_4}$, g=4), and Decocube ($\mathbf{S_5}$, g=5).

C. Adaptive V-Cycle Remeshing

Halfedge Data Structure

The halfedge data structure, illustrated in **Figure 5**, is an efficient and versatile data structure for triangular meshes $\Sigma = (v, h, e)$, where v, e, and f represent vertices, edges, and faces, respectively. Each edge is split into two directed halfedges denoted as h and h_{dual}, linked to associated vertices, edges, faces, and neighboring halfedges, enabling seamless connectivity. This structure excels in localized operations, such as iterating around vertices or faces, which are crucial for tasks like remeshing and curvature computation [**? ?**]. Its balance of efficiency, flexibility, and ease of use makes it indispensable for advanced mesh processing.

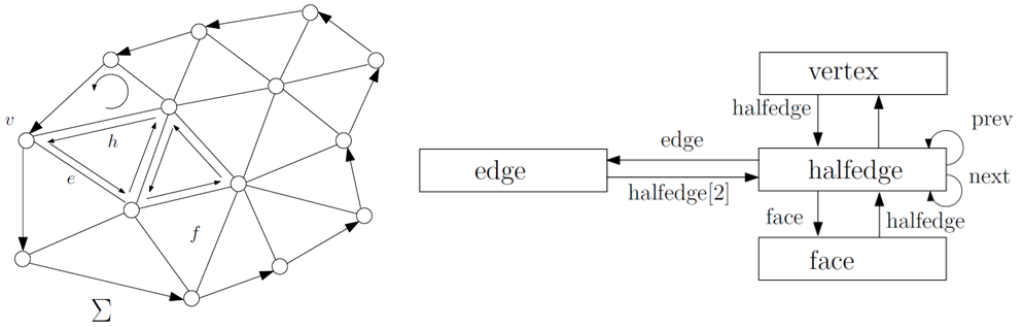

Figure 5. The triangular surface on the left is equipped with a **Half-Edge Data Structure**, illustrated on the right, to enable efficient local mesh operations.[**?**]

Adaptive (Curvature-Guided) Remeshing

Given a triangular mesh $M = (V, E, F)$, where V, E, and F represent vertices, edges, and faces, respectively, adaptive remeshing leverages principal curvatures κ_1 and κ_2 at each vertex $v \in V$ to guide the process. Unlike Isotropic remeshing, which relies on the average edge length $\ell_{\text{avg}} = \frac{1}{|E|} \sum_{e \in E} \|e\|$, adaptive remeshing adjusts edge operations based on curvature, refining high-curvature regions and coarsening flat areas. **Figure 6** contrasts isotropic and adaptive remeshing qualitatively.

Figure 6. Qualitative comparisons between isotropic remeshing and **adaptive(curvature-guided) remeshing**, highlighting finer resolutions in **high-curvature** regions and coarser resolutions in **low curvature** regions.

C2. Pseudo Code for Adaptive V-Cycle Remeshing

Algorithm 1: Gradient Descent with Adaptive V-Cycle Remeshing and Topological Initialization

Input: Mesh $M = (V, E, F)$, learning rate η, remeshing frequency f, maximum iterations T
Output: Optimized vertex positions x^*
Compute the **Euler characteristic** $X(M) = |V| - |E| + |F|$;
Determine the **genus** of the mesh using $g = (2 - X(M))/2$;
Select a triangulated topological primitive with **genus** g (e.g., ranging from 0 to 5) as the initial mesh $M = (V, E, F)$;
Initialize vertex positions x_0 from M;
Set isCoarse $\leftarrow$ True;
for $t = 0$ *to* $T - 1$ **do**
  if $t \mod f == 0$ **then**
    Compute mean curvature H and Gaussian curvature K at each vertex of M;
    Compute principal curvatures κ_1, κ_2 at each vertex using H and K;
    if *isCoarse* **then**
      $x \leftarrow$ Perform Adaptive V-Cycle Remeshing on M with Coarse Resolution using (κ_1, κ_2);
      Set isCoarse $\leftarrow$ False;
    else
      $x \leftarrow$ Perform Adaptive V-Cycle Remeshing on M with Fine Resolution using (κ_1, κ_2);
      Set isCoarse $\leftarrow$ True;
  Compute the loss function $L(\Phi(x))$;
  Compute gradient $\nabla_x L(\Phi(x))$;
  Update vertex positions: $x \leftarrow x - \eta \nabla_x L(\Phi(x))$;
return x^*;

Implementation Details. Our implementation leverages an adaptive curvature-guided remeshing algorithm developed in C++ using the **Half-Edge data structure**, building upon the foundational isotropic remeshing algorithm presented by Botsch *et al.* [**?**] with modifications that enhance adaptability and performance across diverse scenarios. We use principal curvature to guide the remeshing process, enabling accurate capture of geometric details in complex surfaces. In many applications, adaptive remeshing can utilize other metrics for guidance, such as Von Mises stress in elasticity, energy release rates in fracture mechanics, and high-pressure regions in fluid dynamics. This flexibility allows our approach to be tailored to specific engineering needs, ensuring improved simulation accuracy and computational efficiency across various domains.

D. Quantitative Comparison Results for Low and High Genus Surfaces

D1. Quantitative Comparison Results with Nicolet et al.[?] for Low Genus Surfaces

Table 1. Quantitative comparison with Nicolet et al. [**?**] for multi-view reconstructed **low-genus (genus 0)** surfaces: Lower **Chamfer Distance** values mean better results, while higher **Volume IoU** values mean better results. The **Euler characteristic** $\chi(S) = |V|+|F|-|E|$ and the **genus** g are used to evaluate topological consistency, where g represents the number of holes or tunnel loops in the reconstructed surface. Consistent **genus** g numbers indicate that the reconstructed surfaces match the topology of the target surfaces.

	Chamfer Dist ↓	Volume IoU ↑	$\|V\|$	$\|E\|$	$\|F\|$	$\chi(\mathbf{S}) = \|V\| + \|F\| - \|E\|$	**g**
Nicolet et al. [?]							
Armadillo	0.0018	0.8968	112,543	337,623	225,082	2	0
Bunny	0.0021	0.8263	140,607	421,815	281,210	2	0
Nefertiti	0.0018	0.8768	138,695	416,079	277,386	2	0
Planck	0.0019	**0.9369**	146,027	438,075	292,050	2	0
Mario	**0.0024**	0.8683	155,211	465,627	310,418	2	0
Lion	0.0019	0.6685	186,481	559,437	372,958	2	0
Ours (Hybrid)							
Armadillo	**0.0015**	**0.9283**	137,394	412,176	274,784	2	0
Bunny	**0.0020**	**0.8296**	152,642	457,920	305,280	2	0
Nefertiti	**0.0017**	**0.9158**	329,304	987,906	658,604	2	0
Planck	**0.0018**	0.9261	436,224	1,308,666	872,444	2	0
Mario	**0.0024**	**0.9003**	79,032	237,090	158,060	2	0
Lion	**0.0018**	**0.6835**	17,594	52,776	35,184	2	0

D2. Quantitative Comparison Results with Nicolet et al.[?] for High Genus Surfaces

Table 2. Quantitative comparison with Nicolet et al. [**?**] for multi-view reconstructed **high-genus** surfaces: Lower **Chamfer Distance** values mean better results, while higher **Volume IoU** values mean better results. The **Euler characteristic** $\chi(S) = |V|+|F|-|E|$ and the **genus** g are used to evaluate topological consistency, where g represents the number of holes or tunnel loops in the reconstructed surface. Consistent **genus** g numbers indicate that the reconstructed surfaces match the topology of the target surfaces.

	Chamfer Dist ↓	Volume IoU ↑	$\|V\|$	$\|E\|$	$\|F\|$	$\chi(\mathbf{S}) = \|V\| + \|F\| - \|E\|$	**g**
Nicolet et al. [?]							
Kitten	0.0039	0.6298	134,761	404,283	269,522	0	1
Amphora	0.0054	0.4581	91,014	273,048	182,032	2	2
Pretzel	0.0040	0.6518	73,059	219,189	146,126	4	3
Birthay	0.0020	0.4914	28,442	85,344	56,896	6	4
Sorter	0.0672	0.2901	84,189	252,591	168,394	8	5
Ours (Hybrid)							
Kitten	**0.0025**	**0.7126**	15,638	46,914	31,276	0	1
Amphora	**0.0033**	**0.7924**	15,554	46,668	31,112	2	2
Pretzel	**0.0025**	**0.8639**	150,735	452,217	301,478	4	3
Birthay	**0.0006**	**0.8849**	10,197	30,609	20,406	6	4
Sorter	**0.0040**	**0.7504**	298,083	894,273	596,182	8	5

D.3 Quantitative Comparison Results with Nicolet et al.[?] for Challenging High Genus Surfaces

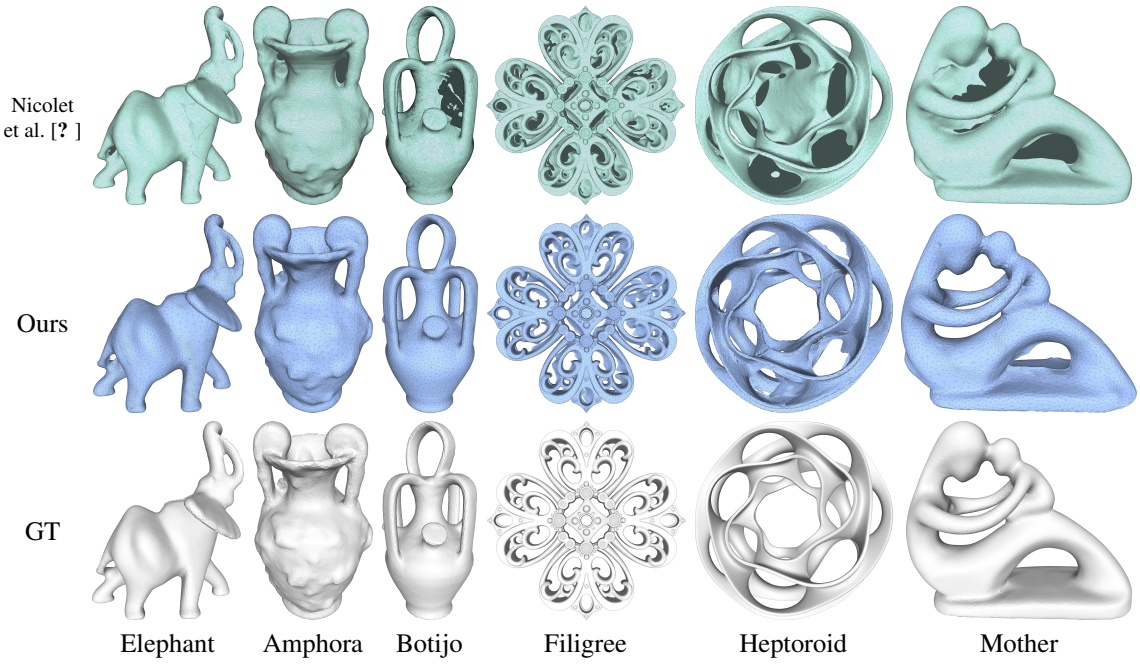

Table 3. Quantitative comparison with Nicolet et al. [?] for multi-view reconstructed **Challenging high-genus** surfaces: Lower **Chamfer Distance** values mean better results, while higher **Volume IoU** values mean better results.

Model	**Chamfer Dist ↓**		**Volume IoU ↑**	
	[?]	**Ours**	[?]	**Ours**
Elephant	0.0035	**0.0008**	0.5297	**0.7606**
Amphora	0.0062	**0.0031**	0.4271	**0.7443**
Botijo	0.0053	**0.0032**	0.4541	**0.8192**
Filigree	0.0019	**0.0018**	0.7365	**0.8204**
Heptoroid	0.0074	**0.0029**	0.5642	**0.8297**
Mother	0.0060	**0.0046**	0.4766	**0.5025**